J MATER SCI 41 (2006) 621–630

Effect of product form and heat treatment on the crystallographic texture of austenitic Nitinol

S. W. ROBERTSON
Department of Materials Science and Engineering, University of California, Berkeley, CA 94720-1760, USA

X. Y. GONG
Nitinol Devices & Components, 47533 Westinghouse Drive, Fremont, CA 94539, USA

R. O. RITCHIE*
Department of Materials Science and Engineering, University of California, Berkeley, CA 94720-1760, USA
E-mail: roritchie@lbl.gov

The superelastic material Nitinol, a nearly equiatomic alloy of nickel and titanium, is rapidly becoming one of the most important metallic implant materials in the biomedical industry, especially for the fabrication of endovascular stents. The manufacture of these stents, and countless other Nitinol products, originates from various forms of raw material such as tube, sheet or rod. However, depending upon which product form is used, the crystallographic texture in Nitinol can be significantly different, which can lead to marked changes in its mechanical properties. In this paper, we present a study to show the characteristic texture in various Nitinol product forms (tube, sheet, and rod), before and after annealing heat treatments, with specific quantification of the major texture components. We further present predictions of the mechanical response based upon such texture, and provide experimental verification with uniaxial tensile tests. Results show that the form of the starting material has a profound influence on characteristic texture and predicted mechanical response. Furthermore, annealing heat treatments, rather than reducing the texture, are found to increase the strength of this texture.

1. Introduction

When conventional engineering materials, such as stainless steel, are mechanically loaded, they undergo typically less than 1% elastic deformation (which is completely recoverable), followed by plastic deformation (which is permanent). Nitinol, a nearly equiatomic nickel-titanium alloy, responds differently; its elastic response is followed by a stress-induced phase transformation from a cubic (austenite) phase to a monoclinic (martensite) phase that can result in fully recoverable macroscopic strains as high as 8% or more. On unloading, the martensite becomes unstable and fully transforms back to austenite, with a concomitant macroscopic strain recovery phenomenon referred to as superelastity. As these martensitic phase transformations depend on coordinated atomic movements, any significant alignment of the atomic planes, i.e., texturing, in the polycrystalline material can have a marked influence on the mechanical response by either limiting or promoting the transformation.

Previous work [1–13] has shown that, in drawn and heat-treated sheet or bar, the mechanical properties of Nitinol are strongly influenced by the texture. In particular, Gall and Sehitoglu [7] concluded that texture, and consequently the martensite variants active during the transformation, are the source of the compression-tension asymmetry in Nitinol. Similarly, Gao and Yi [13] demonstrated a marked influence of texture on the elastic modulus, transformation stress, and transformation strain in

*Author to whom all correspondence should be addressed.
0022-2461
DOI: 10.1007/s10853-006-6478-y

Nitinol, and Vaidyanathan *et al*. [9] showed that texturing occurs in Nitinol only when martensite is stress-induced from austenite. Despite the obvious significance of texture on the mechanical performance of Nitinol, there have been few studies that quantify this texture, particularly in tubing that is used in one of the most important applications of the alloy, that of the manufacture of endovascular stents and other biomedical devices [14].

Accordingly, it is the objective of the present study to seek further understanding of how processing and heat treatment can affect the texture in Nitinol, specifically by quantifying the texture of a variety of raw material forms and heat treatments. The motivation for this investigation is to provide a comparison of the texture of the Nitinol tubes that are used in the fabrication of many biomedical devices (e.g., stents, vena cava filters) with other product forms (sheet and rod), and to determine if annealing heat treatments can be utilized to change the strength and orientation of the texture in order to vary the mechanical response.

2. Experimental procedures

2.1. Material

Nitinol (Ti, 50.8 at.% Ni) in the form of tubing, sheet, and rod was received from Nitinol Devices & Components, Inc. (NDC, Fremont, CA). All samples were processed from multi-vacuum-arc remelted (VAR) material and had an austenite transformation finish temperature (A_f) of 30°C or below. Accordingly they were fully austenitic at ambient temperature during the collection of pole figures. The specific transformation temperatures for each raw material form are given in Table I.

The thin-walled tube was received in two conditions: (a) as-received (drawn plus straightened via thermomechanical processing) with dimensions 4.6 mm outer diameter and 3.9 mm inner diameter, and (b) flattened (described below in Section 2.3). The sheet was received as 0.90-mm thick, as-rolled material. Two rod samples were also obtained from NDC with diameters of 16 and 41 mm. The 16 mm diameter is the predecessor to the deep-drawn tubing described above, whereas the 41 mm diameter material is similar to the Nitinol rods that are being proposed for use in structural applications, such as earthquake-proofing civil structures.

The effect of annealing heat treatments on the tube and sheet was studied using as-received materials that were processed to the following conditions:

- *"485" condition:* as-received tube was reheated for 5 min at 485°C (~0.5 T_m, where T_m is the melting temperature) in an air furnace, followed by an ice-water quench. This heat treatment is common in the Nitinol industry and serves only to stress relieve, slightly lower the tensile strength, and slightly raise the A_f.
- *"850" condition:* as-received Nitinol was annealed *in vacuo* at 850°C (~0.7 T_m) for 30 min followed by a slow cool (10°C per min). This heat treatment does not fully normalize the microstructure, but is used here as it represents a typical industry anneal for studying large-grain phenomena.
- *"1100" condition:* as-received Nitinol was annealed *in vacuo* for 12 h at 1100°C (~0.85 T_m), followed by an ice-water quench. The rationale for this heat treatment was to relieve processing residual stresses, to recrystallize the material, and to eliminate the R-phase.

Optical micrographs of the microstructures of each raw material form and heat treatment are presented in Fig. 1. Several of these show the presence of martensitic grains

TABLE I Transformation temperatures and average grain sizes for the eight sample conditions considered in this study

		Transformation temperatures* (°C)					
Condition	R_s	R_f	M_s	M_f	A_s	A_f	Ave. Grain Size (μm)
Tube							
485°C, 5 min	22	0	−47	−90	16	28	25**
850°C, 30 min	0	−27	−54	−68	−8	4	40
1100°C, 720 min	n/a	n/a	−52	−72	−42	−29	75
flattened	25	13	−26	−63	12	26	25
Sheet							
0.90 mm, 485°C, 5 min	13	5	25	3	13	30	50**
0.90 mm, 850°C, 30 min	−35	−6	−57	−76	−7	2	75
Rod							
16 mm ϕ	−60	−32	−58	−90	−35	−20	90
41 mm ϕ	23	11	−27	−55	14	30	90

*Determined by Differential Scanning Calorimetry (tangent intercept method). R_s, R_f, M_s, M_f and A_s, A_f are, respectively, the orthorhombic *R*-phase, martensite and austenite start and finish temperatures.

**These grain sizes represent the optical microscope resolved dimensions. Transmission electron microscopy above 50,000× magnification reveals a sub-grain structure of ~10 nm average size, which are annihilated at the higher temperature heat treatments [14].

(needle-like appearance); however, these are polishing artifacts as the stresses from grinding and polishing cause transformation in exposed grains which leaves residual surface relief on etching. Moreover, the apparent grain sizes of ∼20 μm, observed with optical microscopy for the "485" conditions, also give a false impression; there exist much smaller "sub-grains" (∼10 nm) that can only be revealed by transmission electron microscopy [14].

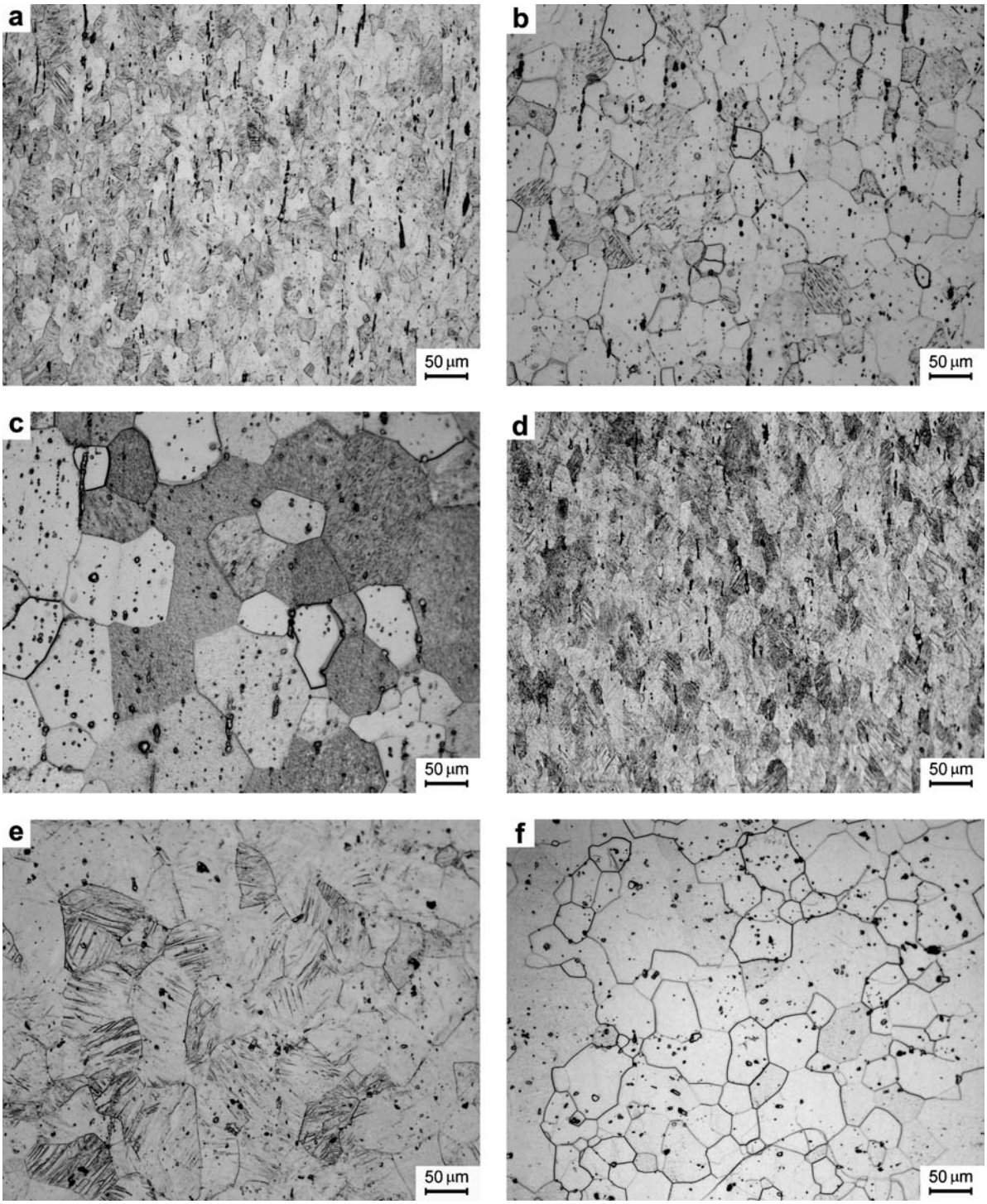

Figure 1 Photo-micrographs of the eight raw material forms in this study, (a) tube, 485°C (∼0.50 T_m), 5 min, quench, (b) tube, 850°C (∼0.70 T_m), 30 min, −10°C/min, (c) tube, 1100°C (∼0.85 T_m), (d) tube, flattened through a five-step thermo-mechanical shape-setting process, (e) 0.90 mm thick sheet, 485°C (∼0.50 T_m), 5 min, quench, (f) 0.90 mm thick sheet, 850°C (∼0.70 T_m), 30 min, −10°C/min, (g) 16 mm diameter rod, no heat treatment, (h) 41 mm diameter rod, no heat treatment. Etchant: 3.2% HF, 14.6% HNO_3, balance deionized water. The drawing/rolling direction is vertical.

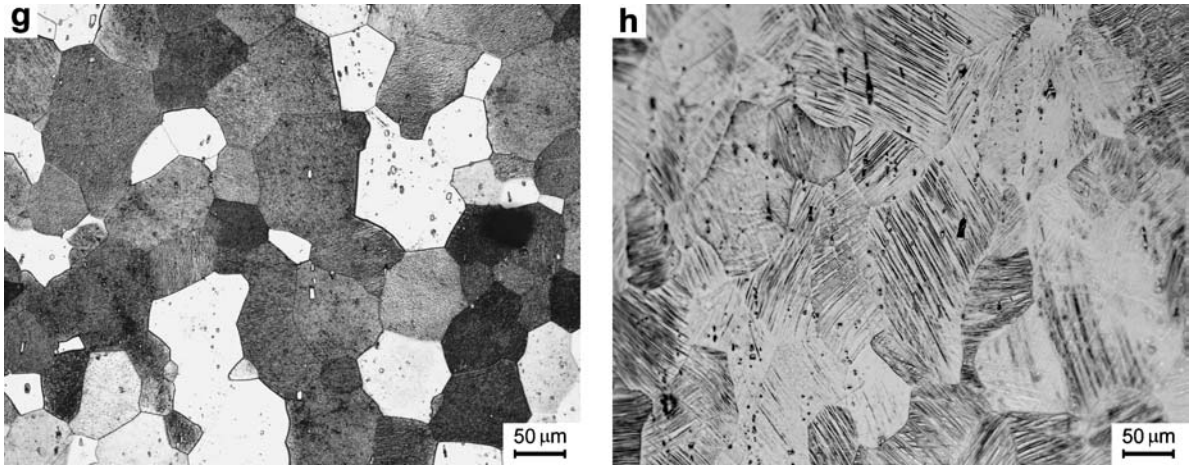

Figure 1 Continued.

2.2. Characterization

Textures were measured in reflection geometry with a Huber X-ray pole figure goniometer, with Cu-Kα radiation source at 40 kV and 14 mA, and a graphite monochromator. To provide large enough flat samples, the tubes were sliced into sections, the sections were then lined up side-by-side to form an approximate 10 mm square, cold-mounted in epoxy and polished flat. All tube and sheet samples were mechanically ground and polished to a 0.05 μm finish to permit optimal reflective X-ray diffraction and establish consistency among the samples. The rod samples were longitudinally laser cut and electropolished to remove any machining effects. All samples were heated to $\sim$50°C prior to testing and slow cooled back to room temperature to ensure they were fully austenitic throughout the test.

The crystallographic texture of the Nitinol was determined from three "incomplete measured" pole figures, namely the 110, 200 and 211 diffraction peaks, at θ values of, respectively, 21.3°, 30.8° and 38.9° for Cu-Kα radiation, where θ is half of the angle between the incident X-rays and the detector. The raw intensities were corrected for background and defocusing and only data out to a maximum tilt angle distance of 65° were used. The Williams-Imhof-Matthies-Vinel (WIMV) algorithm [15], which calculates orientation distributions from pole figures, was employed in the BEARTEX software package for quantitative texture analysis in order to obtain the orientation distribution functions (ODF) [16]. From the ODF, pole figures and inverse pole figures were recalculated following standard smoothing and rotation operations. The smoothing operation was performed mainly to reduce the effects (if any) of highly oriented single crystals in the bulk sample. Rotation was necessary to orient each pole figure in the sample reference orientation for comparison among the samples. This reference orientation is illustrated in Fig. 2.

Except for the flattened tube, the experimental pole figures for the Nitinol tube samples represent the average of three separate tests. For the Nitinol sheet, rod, and flattened tube samples, only one test was used in the texture analysis because of limited sample supply. However, each sample was tested multiple times and yielded nearly identical results each time.

2.3. Mechanical testing

In order to evaluate the mechanical response of Nitinol tubing by uniaxial tensile testing, Nitinol tubing was flattened so that dog-bone shaped samples could be produced at various angles to the drawing axis. The tensile specimens were fabricated by the following procedures:

(a) Superelastic Ti-50.8Ni (at.%) tubing with 5.84 mm OD $\times$ 4.98 mm ID was laser cut longitudinally so the tube could be uncurled.
(b) Laser cut pieces were then flattened through a series of five thermo-mechanical shape-setting procedures to form flat strips of 76.2$\times$17.0 mm.
(c) Resulting flat strips were tuned to produce an A_f of 28°C.
(d) After heat treatment, the strips were laser cut to form dog-bone shaped test samples parallel to the longitudinal, circumferential, 22.5°, 45°, and 67.5° tube directions. Dog-bone gauge dimensions were nominally 0.75 mm wide, 0.40 mm thick, and 7.5 mm long.
(e) Laser cut samples were microblasted and electropolished to remove the laser-affected zone and to achieve a uniform surface finish and passive oxide.

Uniaxial tensile testing was performed on an EnduraTEC/BOSE desktop tester ELF3200 (ELectroForce) series. A customized air-heating chamber was used to maintain a temperature of 37°C during testing at a crosshead displacement rate of 4.0 μm/sec to ensure

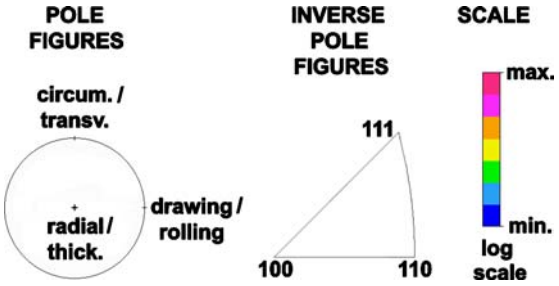

Figure 2 Legend for the pole figures (stereographic projection) and inverse pole figures (equal area projection). Intensities for every texture figure in this text are plotted on the same logarithmic scale from 100 (min) to 600 (max).

adiabatic conditions. Strains were determined from a miniature extensometer with gauge length of 3 mm.

3. Results and discussion

3.1. Comparison of product forms

To determine the role of product form, pole figures and inverse pole figures for tube, sheet, and rod with nominally similar heat treatment were compared. Using Fig. 2 to define the legends for all pole figures and inverse pole figures shown in this paper, it is apparent from Fig. 3 that although the intensity, or the relative texture strength, is approximately the same, the specific nature of the texture depends markedly on the form of the raw material. The texture of the sheet is characteristic of hot-rolled body-centered-cubic (bcc) materials, as is the 110 fiber texture for the rod [17].

To reproduce the effect of processing that a product may undergo during manufacturing, i.e., through the shape-setting procedure, tube samples were longitudinally cut and flattened. Despite the severity of the flattening process in this sample, the texture of the tube remained relatively constant (Fig. 4). The only significant difference in the "485" versus the flattened tube is the increased 110 radial direction texture strength in the flattened tube.

With the results from the tube showing consistency in texture following mechanical processing, it was quite surprising to discover widely varying textures in rod (Fig. 5) of various dimensions and lots. The texture from two different diameter rods was quite different (Fig. 5). The 16 mm diameter rod, which is the precursor to the deep-drawn tubes that were analyzed previously, exhibited a higher texture strength and different localized texture components than the 41 mm rod. Comparison of the 16 mm diameter rod texture (Fig. 5) with that of the "485" tube (Fig. 4) shows distinctly different textures following the processing. It is interesting that the severe process of deep-drawing a rod into a tube shape has a profound impact on the texture, whereas the process of flattening or uncurling the tube resulted in minimal textural changes. This observation suggests that although the form of the starting material has a marked effect on the texture, the shape setting procedures produce little change. These results are of significance for biomedical Nitinol components, as most manufacturers use some form of shape setting or material "training" during processing.

3.2. Heat treatment comparison

As most biomedical Nitinol products undergo some form of heat treatment to "tune" the transformation temperatures, it is important to understand the effect of such treatments on the texture of Nitinol. In the present work, the effect of annealing heat treatments was largely performed on tubular raw material form, which is most widely used in the biomedical community, although sheet samples were also examined for comparison.

Unlike many engineering alloys that normalize, or randomize, their grain structure following annealing heat treatments at high homologous temperatures (up to $T/T_m \sim 0.85$) the strength of the texture in Nitinol was found to be increased. This is indicated by the progressively higher intensity (relative density of red in the pole figures) as the annealing temperatures and times increase (Fig. 6). The inverse pole figures demonstrate a progressive redistribution of texture from 111 poles in the radial direction and both 111 and 110 poles in the drawing direction in the "485" condition, to 110 radial and 111 drawing direction textures. Except for these differences, the tube texture remains generally similar throughout the heat treatment process.

Sheet material exhibits the same trend of increasing texture intensity with increasing heat treatment (Fig. 7). The sheet texture also redistributes upon heating, although more slightly than the tube, and spreads from predominantly 111 radial poles towards the 110 pole, with the drawing direction texture remaining approximately the same.

Textures measured for Nitinol sheet compare favorably with previous measurements cited in the literature [1, 2, 4], although, to our knowledge, there are no other reported data apart from our own on the texture of Nitinol tubes [14]. Specifically, the current textures for 0.90 mm thick "485" sheet are very similar to those determined by Monasevich *et al*. [1], Li *et al*. [2], and Inoue *et al*. [4] on other Nitinol plate and sheet geometries. However, pole figures derived by Kitamura *et al*. [5] are quite different, presumably because their study was focused on a much thinner (100 μm) Nitinol sheet; they showed a texture maximum of the 110 pole normal to the sheet, which was not observed in the present study.[1]

[1] We have observed such a 110 normal-direction texture in a different Ni-rich (55.5 at.%) Nitinol material processed by both vacuum-induction-melting and vacuum-arc-melting (VIM-VAR). Unlike the multi-VAR material used in the current study, due to interaction with the crucible, the VIM-VAR process leads to a different as-cast structure and a higher carbon content

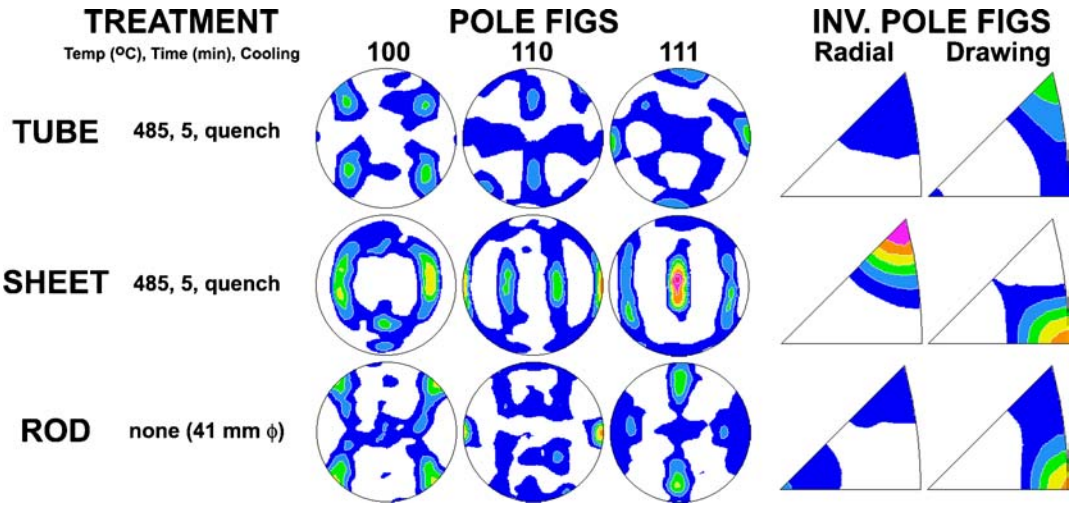

Figure 3 Raw material form texture comparison (tube, sheet, and rod) showing many differences in the orientation distributions in both the pole figures and inverse pole figures.

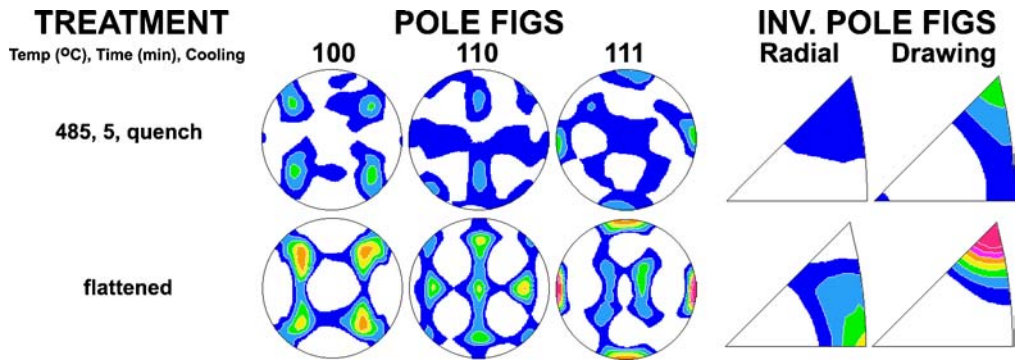

Figure 4 Texture effects as a function of shape-set processing demonstrating that the texture strength increases slightly, but the overall distribution of orientations remains relatively similar.

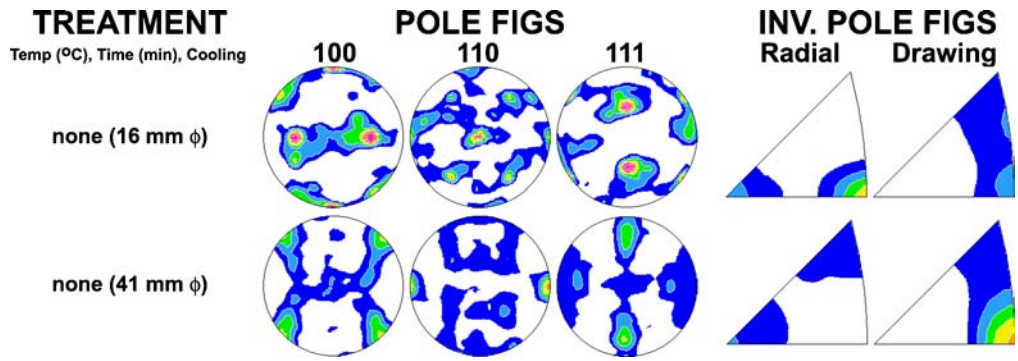

Figure 5 Rod material comparisons showing that the two samples exhibited different orientation distributions; namely the 16 mm rod has a strong 110 radial component, whereas the 41 mm rod has strong 110 drawing direction texture.

3.3. Texture quantification

Quantification of the major components of textures in each set of samples was performed using the BEARTEX software with a component radius of 10°; results are presented in Tables II–IV and show the texture components representing 5% or more of the total volume, with the remainder assumed to be randomly distributed. In these tables, each Euler-angle-described component was approximated as a Miller index pair $\{hkl\}\langle uvw\rangle$ representing the

(0.07 at.% C in this alloy), which may be responsible for the 110 normal-direction texture.

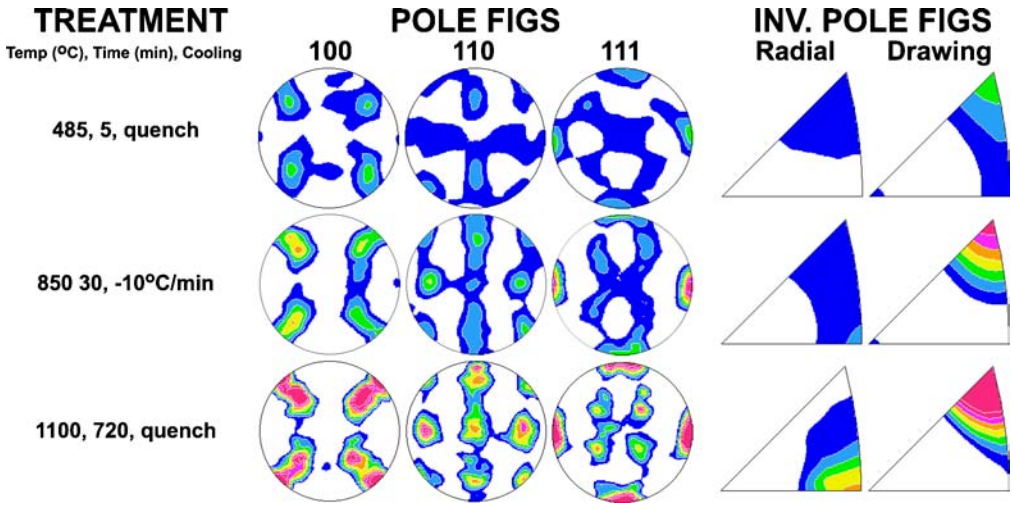

Figure 6 Effect of annealing heat treatment on the texture of Nitinol thin-walled tube showing increasing texture strength and redistribution of radial poles from the 111 to the 110 position with heat treatment.

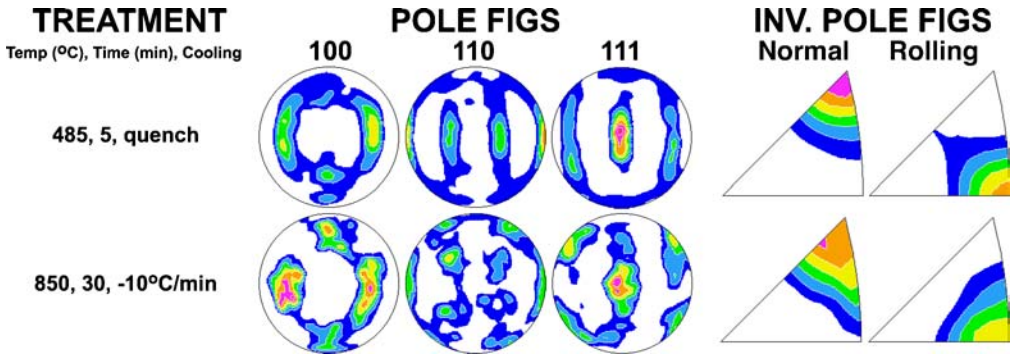

Figure 7 Effect of annealing heat treatment on texture in 0.90 mm thick Nitinol sheet showing general strengthening of texture and a spreading of the 111 normal direction texture with heat treatment.

{hkl} plane families normal to the radial/thickness direction, and ⟨uvw⟩ direction families parallel to the drawing/rolling direction.

Table II shows that each of the tube samples could be described by a combination of five crystalline components, with the $\{221\}\langle 1\bar{2}2\rangle$ strongest in every sample. Two ⟨111⟩ drawing direction components, namely the {110} and {112} planes, combined to greater than or equal to the strength of the $\{221\}\langle 1\bar{2}2\rangle$ single component and accounted for the strong 111 pole in the tube drawing direction inverse pole figures. In addition to the relative similarity in the major textural components is an increase in the volumetric percent of each texture component upon heat treatment; the "485", "850" and "1100" samples have texture volume percentages of 45, 59, and 73% respectively. This trend indicates a structured recrystallization upon heat treatment. An increase in texture strength, though no significant change in orientation, was also noted following the flattening process and is attributed to the heat treatments necessary to shape-set the tube to a flattened configuration.

TABLE II Quantified textures for tube raw material form showing the principal texture component of $\{221\}\langle 1\bar{2}2\rangle$ in each sample, plus secondary 111 drawing direction texture components

Component Euler angles (α, β, γ)	Approx. Miller index {hkl}⟨uvw⟩	Volume percent			
		485°C, 5 min	850°C, 30 min	1100°C, 12 hr	Flat
315, 70, 45	$\{221\}\langle 1\bar{2}2\rangle$	16	19	22	20
35, 45, 0	$\{110\}\langle 1\bar{1}1\rangle$	8	12	16	14
0, 35, 45	$\{112\}\langle 11\bar{1}\rangle$	8	13	13	12
325, 90, 45	$\{110\}\langle 1\bar{1}2\rangle$	5	9	15	10
270, 35, 45	$\{112\}\langle 1\bar{1}0\rangle$	8	6	7	8

Like the tubes, the sheet samples (Table III) produced similar increased texture volume percentages with increasing heat treatment time and temperature; the sheet increased from 45% total texture in the "485" to 57% texture in the "850" sample. Both samples show predominantly ⟨110⟩-type rolling texture which is consistent with an α-fiber rolling texture for bcc materials [17]. The

TABLE III Quantified textures for sheet raw material form demonstrating the principal 110 drawing direction texture consistent with an α-fiber texture in bcc materials

Sheet condition	Component Euler angles (α, β, γ)	Approx. Miller index {hkl}⟨uvw⟩	Vol.%
0.90 mm thick, 485°C, 30 min	60, 45, 45	$\{111\}\langle 11\bar{2}\rangle$	17
	270, 45, 45	$\{223\}\langle 1\bar{1}0\rangle$	15
	270, 75, 45	$\{221\}\langle 1\bar{1}0\rangle$	13
0.90 mm thick, 850°C, 5 min	30, 55, 45	$\{111\}\langle 1\bar{1}0\rangle$	27
	0, 45, 0	$\{110\}\langle 1\bar{1}0\rangle$	18
	90, 70, 45	$\{221\}\langle 1\bar{1}0\rangle$	6
	270, 65, 30	$\{211\}\langle 1\bar{2}0\rangle$	6

strongest normal direction component, i.e. the plane parallel to the rolling direction, was the {111} in both sheet samples.

Approximately 60% of the 16 mm diameter rod crystallites were represented by two simple crystallite orientations, $\{110\}\langle\bar{1}10\rangle$ and $\{100\}\langle 011\rangle$ (Table IV), indicating a strong 110 drawing direction texture. Conversely, the larger 41 mm diameter rod exhibited a more even distribution of five different texture components. The majority of these components also exhibited 110 drawing direction texture. Although the two tubes analyzed here show consistent drawing direction texture, they differ from the recent work by Frick *et al.* [18] who demonstrated a 111 drawing direction texture. These differences are most likely caused by variations in the manufacturing of each rod, e.g., deep drawing vs. rotary forging.

In light of these findings, it is clear that selection of the appropriate raw material product form is critical to obtaining accurate mechanical test results when characterizing Nitinol materials, particularly in proof testing for quality assurance. In addition, a critical finding is that *the texture of Nitinol materials cannot be removed, or even reduced, in these product forms using standard annealing or normalization heat treatment procedures*.

TABLE IV Quantified textures for rod raw material form with the principal drawing direction texture identified as ⟨110⟩ type texture

Rod condition	Component Euler angles (α, β, γ)	Approx. Miller index {hkl}⟨uvw⟩	Vol. %
15 mm ϕ	0, 45, 0	$\{110\}\langle 1\bar{1}0\rangle$	45
	45, 90, 0	$\{100\}\langle 011\rangle$	18
41 mm ϕ	46, 90, 15	$\{130\}\langle 3\bar{1}3\rangle$	13
	30, 55, 45	$\{111\}\langle 1\bar{1}0\rangle$	11
	220, 75, 20	$\{113\}\langle 1\bar{1}0\rangle$	8
	45, 90, 0	$\{100\}\langle 011\rangle$	6
	0, 45, 0	$\{110\}\langle 1\bar{1}0\rangle$	5

3.4. Mechanical behavior

To demonstrate the effect of texture on the mechanical properties of Nitinol, the strains at the end of the transformation stress plateau (i.e., on the stress/strain curve) were estimated. Following the technique of Yuan and Yi [8] for textured Nitinol sheet, this transformation strain can be calculated from the modified Taylor factors derived by Ono *et al.* [19, 20] for polycrystalline Nitinol. Specifically, using optimization algorithms for the formation of the twelve variants of martensite, Ono *et al.* created a modified Taylor factor, M', distribution map, as shown in Fig. 8, which shows modified Taylor factors as a function of the texture in the tensile loading direction. Using this map and the inverse pole figures determined from the current experimental data, the transformation strain, ε, was calculated from:

$$\varepsilon = \frac{\eta V_{\mathrm{m}}}{M'_{\mathrm{ave}}}, \tag{1}$$

where η is the maximum habit plane displacement magnitude (=13.08 from ref. [20]), V_{m} is the volume fraction of martensite (=1.00 for 100% conversion in this case), and M'_{ave} is the average modified Taylor factor:

$$M'_{\mathrm{ave}} = \frac{\int (E(h,k,l) \times M'(h,k,l))}{\int E(h,k,l)}, \tag{2}$$

where $E(h, k, l)$ is the discrete texture intensity at a given (h, k, l) Miller index position on the experimentally measured inverse pole figures, and $M'(h, k, l)$ is the corresponding modified Taylor factor intensity from Fig. 8. Thus, M'_{ave} represents the normalized Taylor factor for each specific polycrystalline form of Nitinol in this study.

Inverse pole figures were produced for the flattened tube for inclined sample directions between 0 and 90 degrees, in 5 degree increments, with respect to the drawing direction. These inverse pole figures provided the

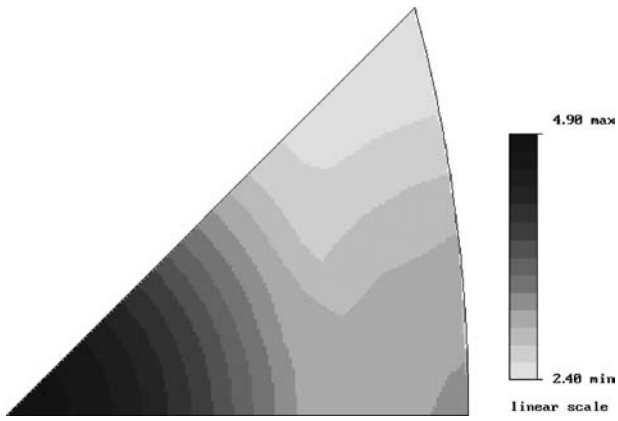

Figure 8 Modified Taylor factor distribution, M', after Ono *et al.* [20] showing the factor as a function of texture and tensile loading direction.

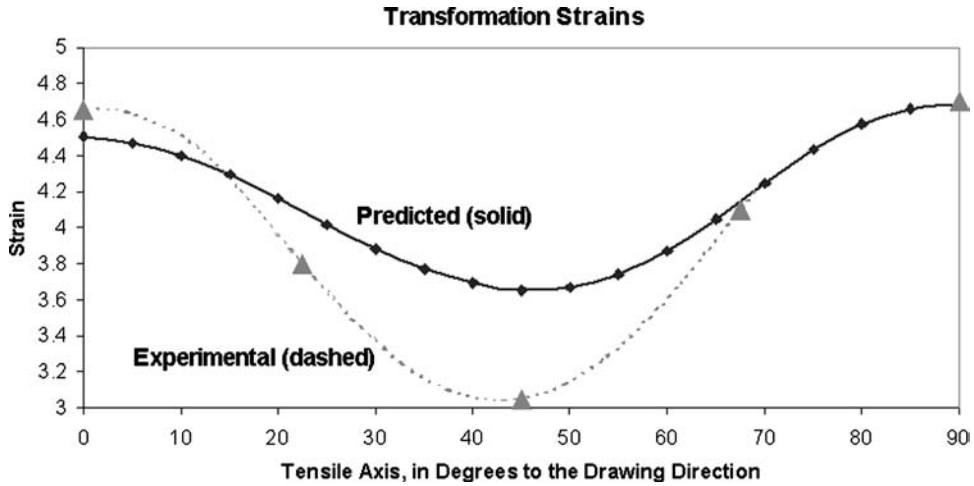

Figure 9 Texture-predicted transformation strains versus loading angle relative to the drawing axis for flattened tube (solid line), with experimentally determined (by uniaxial tension tests) transformation strains (dashed line) showing good correlation; 16% maximum difference at 45°.

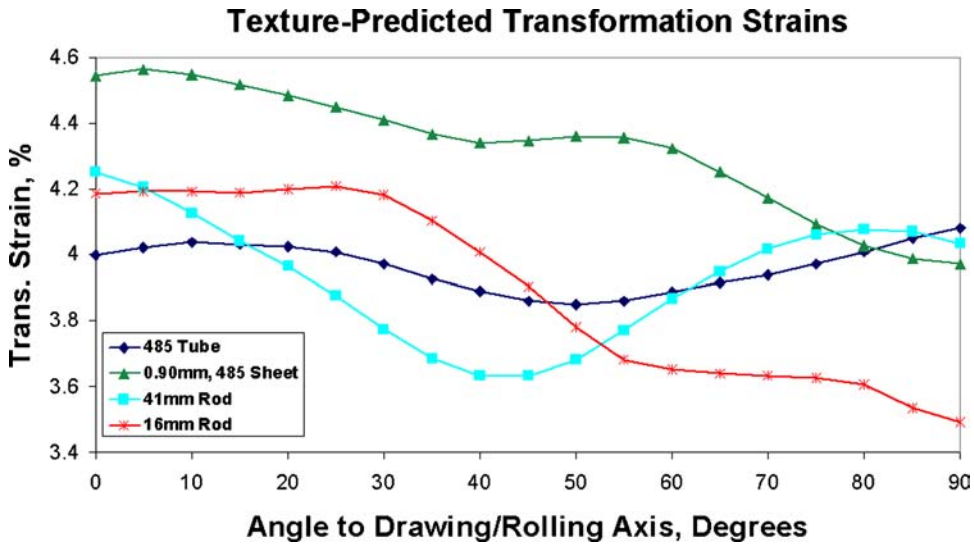

Figure 10 Texture-predicted transformation strains versus loading angle relative to the drawing direction for tube, sheet, and rod Nitinol raw material forms.

necessary $E(h, k, l)$ distributions to predict the flattened tube transformation strain as a function of applied load direction. The transformation strain predictions are plotted in Fig. 9, and clearly show that a lower strain is necessary for complete transformation when the sample is loaded parallel to the 45° direction. The transformation strains from our laboratory uniaxial tension experiments follow the same general trend as this predicted mechanical response. The discrepancy is surprisingly small, namely 16% maximum. The good agreement indicated that the modified Taylor factor calculations are a very good estimation to predict the transformation strain from the determined Nitinol texture. It is also of note that these predicted results are consistent with paths of fatigue cracks in this material which, irrespective of the path of maximum driving force, preferentially follow the 45° direction, i.e., that of lowest required strain energy to form martensite.

Finally, Fig. 10 shows the predicted transformational strains of the tube, sheet and rod raw material forms that are commonly used for industrial Nitinol products. The wide variability in the transformation strains for tube, rod and sheet demonstrates the need for quantification of texture in every raw material form appropriate for each Nitinol supplier and manufacturer.

4. Conclusions

Nitinol derives its unique mechanical behavior from the coordinated atomic movements manifesting in a phase transformations from cubic austenite to monoclinic martensite. Therefore, any significant alignment of the atomic planes from texture in the polycrystalline material can have a marked influence on the mechanical response by either limiting or promoting that phase transformation.

The texture analysis presented in this paper has shown that Nitinol does exhibit crystallographic orientation resulting from its forming and processing, which cannot be eliminated by annealing at high homologous temperatures up to ~0.85 T_m. Interpretation and quantification of the pole figures and inverse pole figures leads to the following specific conclusions:

(1) Each material product form (tube, sheet and rod) possesses a unique characteristic texture. Indeed, even rods of different diameter have different textures.

(2) Annealing Nitinol tube and sheet for increasing time and temperature increases the crystallographic alignment in the sample. The location of the texture components, i.e., the Miller index quantification, however, remains somewhat constant upon continued annealing despite the increasing volume percent of textured grains. The texture of these tubes was characterized by the principal component $\{221\}\langle 1\bar{2}2\rangle$ with secondary$\langle 111\rangle$ drawing direction components equaling or surpassing the principal component contribution.

(3) Shape-setting of tubular Nitinol does not significantly affect the major texture component identity, and serves to only slightly increase the texture intensity. The only significant difference after the severe shape setting process of flattening a tube was found to be the increased 110 radial direction texture strength.

(4) The texture of 16 mm diameter rod was highly oriented; specifically, 60% of the grains were oriented with 110 drawing direction texture. The manufacturing step of producing tubes from this rod via a deep-drawing step significantly changed the texture and introduced a more evenly distributed texture over several components.

(5) Experimental transformation strains were in good agreement with modified Taylor factor calculations for transformation to the twelve variants of martensite. These predictions and mechanical tests show that the transformation strain for Nitinol tube is lowest at a loading direction approximately 45° to the drawing direction, and that texture in various raw material forms has a profound influence on the transformation strains.

Acknowledgements

This work was supported by the National Science Foundation under Grant No. CMS-980006, and by a gift from Nitinol Devices and Components (NDC, Inc., Fremont, CA). The authors would like to thank Dr. Hans-Rudolf Wenk for many helpful discussions and advice. We also acknowledge Drs. Tom Duerig and Alan Pelton of NDC for their continued support and for supplying the Nitinol samples.

References

1. L. A. MONASEVICH, Y. I. PASKAL, V. E. PRIB, G. D. TIMONIN and D. B. CHERNOV, *Met. Sci. Heat Treat.* **21** (1979) 735.
2. D. Y. LI, X. F. WU and T. KO, *Acta Metall. Mater.* **38** (1990) 19.
3. J. H. MULDER, P. E. THOMA and J. BEYER, *Z. Metallkd.* **84** (1993) 501.
4. H. INOUE, N. MIWA and N. INAKAZU, *Acta Mater.* **44** (1996) 4825.
5. K. KITAMURA, S. MIYAZAKI, H. IWAI and M. KOHL, in the Proceedings of the Second International Shape Memory and Superelastic Technologies Conference, Asilomar, edited by A. R. Pelton, D. E. Hodgson, S. M. Russell and T. W. Duerig, CA, USA, March 1997, p. 47.
6. Y. C. SHU and K. BHATTACHARYA, *Acta Mater.* **46** (1998) 5457.
7. K. GALL and H. SEHITOGLU, *Int. J. Plasticity* **15** (1999) 69.
8. W. Q. YUAN and S. YI, *Mater. Sci. Eng. A* **271** (1999) 439.
9. R. VAIDYANATHAN, M. A. M. BOURKE and D. C. DUNAND, *Metall. Mater. Trans. A* **32A** (2001) 777.
10. E. HORNBOGEN, G. BRUCKNER and G. GOTTSTEIN, *Z. Metallkd.* **93** (2002) 3.
11. H. SITEPU, W. SCHMAHL and B. VON DREELE, *Appl. Phys. A* **74** (2002) S1676.
12. J. M. MCNANEY, V. IMBENI, Y. JUNG, P. PAPADOPOULOS and R. O. RITCHIE, *Mech. Mater.* **35** (2003) 969.
13. S. GAO and S. YI, *Mater. Sci. Eng.* **A362** (2003) 107.
14. S. W. ROBERTSON, V. IMBENI, H. R. WENK and R. O. RITCHIE, in Proceedings of the Shape Memory and Superelastic Technologies Conference (Baden-Baden, Germany, 2004) in press.
15. S. MATTHIES and G. W. VINEL, *Phys. Stat. Sol. B* **112** (1982) K111.
16. H. R. WENK, S. MATTHIES, J. DONOVAN and D. CHATEIGNER, *J. Appl. Cryst.* **31** (1998) 262.
17. U. F. KOCKS, C. N. TOME and H. R. WENK in "Texture and Anisotropy" (Cambridge University Press, 1998) p. 195.
18. C. P. FRICK, A. M. ORTEGA, J. TYBER, K. GALL and H. J. MAIER, *Metall. Mater. Trans. A* **35**A (2004) 2013.
19. N. ONO and A. SATO, *Trans. Jpn. Inst. Metals* **29** (1988) 267.
20. N. ONO, A. SATOH and H. OHTA, *ibid.* **30** (1989) 756.